

A Weighted Least-Squares Transport Equation Compatible with Source Iteration and Voids

Hans R. Hammer^{* 1,2}, Jim E. Morel^{† 2}, and Yaqi Wang^{‡ 3}

¹Los Alamos National Laboratory - T3: Fluid Dynamics and Solid Mechanics, Bikini Atoll Road, Los Alamos, NM, 87545

²Texas A&M University - Department of Nuclear Engineering, 3133 TAMU, College Station, TX 77843-3133

³Idaho National Laboratory, 1955 N. Fremont Ave, Idaho Falls, ID 83415

^{*}email: hrhammer@lanl.gov

[†]email: morel@tamu.edu

[‡]email: yaqi.wang@inl.gov

Abstract

Second order forms of the transport equation allow the use of continuous finite elements (CFEM). This can be desired in multi-physics calculations where other physics require CFEM discretizations. Second-order transport operators are generally self-adjoint, yielding symmetric positive-definite matrices, which allow the use of efficient linear algebra solvers with an enormous advantage in memory usage.

Least-squares (LS) forms of the transport equation can circumvent the void problems of other second order forms, but are almost always non-conservative. Additionally, the standard LS form is not compatible with discrete ordinates method (S_N) iterative solution techniques such as source iteration. A new form of the least-squares transport equation has recently been developed that is compatible with voids and standard S_N iterative solution techniques. Performing Nonlinear Diffusion Acceleration (NDA) using an independently-differenced low-order equation enforces conservation for the whole system, and makes this equation suitable for reactor physics calculations. In this context independent means that both the transport and low-order solutions converge to the same scalar flux and current as the spatial mesh is refined, but for a given mesh, the solutions are not necessarily equal.

In this paper we show that introducing a weight function to this least-squares equation improves issues with causality and can render our equation equal to the Self-Adjoint Angular Flux (SAAF) equation. Causality is a principle of the transport equation which states that information only travels downstream along characteristics. This principle can be violated numerically. We show how to limit the weight function in voids and demonstrate the effect of this limit on the accuracy. Using the C5G7 benchmark, we compare our method to the self-adjoint angular flux formulation with a void treatment (SAAF τ), which is not self-adjoint and has a non-symmetric coefficient matrix. We show that the weighted least-squares equation with NDA gives acceptable accuracy relative to the SAAF τ equation while maintaining a symmetric positive-definite system matrix.

Keywords — Neutron Transport, Weighted Least-Squares, Nonlinear Diffusion Acceleration, Voids, HOLO

I. INTRODUCTION

Second order forms of the transport equation offer a stable discretization using continuous finite elements (CFEM), which is especially appealing in the context of multi-physics calculations within frameworks with well-developed support for CFEM. One example is Rattlesnake [1, 2], Idaho National Laboratory’s transport code within the MOOSE framework [3], which supports several second order schemes. Additionally, a second order form is generally compatible with discretizations that result in symmetric positive-definite (SPD) matrices [4] for the standard source iteration equations with S_N discretization. SPD matrices can then be solved by highly efficient linear algebra solvers, especially the conjugate gradient method [5] with preconditioning. The conjugate gradient algorithm only requires the storage of three solutions vectors, which is a large advantage compared with the general GMRES algorithm for non-SPD matrices and thus can also offer better convergence since no restart is necessary.

Current developments in modeling and simulation raised the needs for tools which are able to handle voids or near voids. While this is definitely possible with the first order transport equation, second order schemes often show singularities and conditioning or convergence problems for very small (near zero) total cross sections [6, 7]. Certain least-squares (LS) forms of the transport equation can circumvent the void problems of other second order forms, but are non-conservative, which explains why they are not commonly used in the nuclear community. Additionally, the left-hand side of the standard LS equations are coupled between all directions due to scattering, preventing the use of standard S_N iterative solution techniques. A newly developed form of the least-squares transport equation is compatible with voids and standard S_N iterative solution techniques, but is also non-conservative [8]. Conservation of particles is only achieved as the numerical solution converges to the analytical solution. Conservation is of the utmost importance for criticality calculations, and if not enforced, can lead to large errors in the critical eigenvalue (k_{eff}) [9] and the flux.

Source iteration is a common and well proven method to iteratively solve the discrete ordinates equations [10]. Over the years researchers developed many improvements to this simple solution process. Many addressed the slow iterative convergence of the source iterations for highly diffusive media, for example, via diffusion synthetic acceleration (DSA) or nonlinear diffusion acceleration (NDA). In addition, the use of an inconsistent, but conservative NDA low-order equation enforces conservation for the whole system as shown by Peterson et al. [9] and therefore is an important improvement for the weighted LS equation even in non-diffusive cases. The NDA method is especially of interest for reactor physics problems, since it is easily adopted to solve criticality problems [11], and enforces conservation of particles for the WLS equation. Linear DSA does not seem to be appropriate for criticality problems if one wants to perform the k_{eff} -calculation with the low-order diffusion equations. Voids are problematic for both DSA and NDA because the standard diffusion coefficient is unbounded in voids.

The purpose of this paper is to develop a weighted least-squares transport formulation that is compatible with voids. We have also developed a conservative void-compatible NDA scheme for our weighted least-squares transport formulation. However, in this paper we focus upon our weighted least-squares transport formulation. The void-compatible NDA scheme will be described in a separate paper [12]. Instead we use the conservative NDA scheme of Peterson et al. [9] in this paper, which is not void-compatible.

In this paper we show that introducing a weight function to this LS equation improves issues with causality and can render our equation equal to the Self-Adjoint Angular flux (SAAF) equation [7]. Causality is a principle of the transport equation which states that information only travels downstream along the direction of neutron travel. This principle can be violated numerically. We show how to limit the weight function in voids and the effect of this limit on accuracy. Using the C5G7 benchmark we compare our method against the self-adjoint angular flux formulation with a void treatment (SAAF τ), which was introduced by Wang [2]. This formulation uses a first order derivative for stabilization in optically thin cells, which results in a non-symmetric coefficient matrix. We demonstrate that the weighted least-squares equation with NDA gives acceptable accuracy relative to the SAAF τ equation while maintaining a symmetric positive-definite system matrix.

In the next section we first derive the SAAF τ equation, and show that it can reduce to the first-order equation or the SAAF equation, depending upon the value of a certain parameter. Then we derive our weighted least-squares (WLS) equation, and show that it can reduce to the SAAF equation depending upon the definition of the weight function. Our NDA scheme for the WLS equation is then derived. Computational

results are given in the next section. These results relate to following: a comparison of the weighted and unweighted least-squares equations; limiting of the weight function in voids; and a comparison of the SAAF τ and WLS methods applied to the C5G7 reactor physics benchmark. In the final section we give conclusions and a summary of results.

II. THEORY

II.A. Self-Adjoint Angular Flux Equation with void treatment

The standard SAAF equation [7] is not defined in voids. Wang et al. [2] proposed a modified version of the SAAF equation that is well defined in voids. Here we shall give a short derivation of the self-adjoint angular-flux equation with void treatment (SAAF τ). Further details are described in the paper by Wang. This equation is used as comparison for our WLS equation.

We will derive the steady-state mono-energetic SAAF τ equation for simplicity. The extension to multi-group is straightforward. Consider the first order transport equation in operator form, where $\psi(\vec{x}, \vec{\Omega})$ is the angular flux with $\vec{x} \in \mathcal{D}$, $\vec{\Omega} \in 4\pi$ (4π represents the entire 2D unit sphere)

$$\mathcal{L}\psi = \mathcal{S}\psi + \mathcal{F}\psi + \mathcal{Q} \quad (1a)$$

where

$$\mathcal{L} \equiv \vec{\Omega} \cdot \vec{\nabla} + \sigma_t \quad (1b)$$

is the streaming and collision operator,

$$\mathcal{S} \equiv \sum_{l=0}^{\infty} \sum_{p=-l}^l \frac{2l+1}{4\pi} Y_l^p(\vec{\Omega}) \sigma_l \mathcal{M} \quad (1c)$$

the scattering operator with

$$\mathcal{M} \equiv \int_{4\pi} d\vec{\Omega} Y_l^p(\vec{\Omega}) \quad (1d)$$

the flux moments and the scattering moments

$$\sigma_l \equiv 2\pi \int_{-1}^1 \sigma_s(\mu) P_l(\mu) d\mu. \quad (1e)$$

Finally

$$\mathcal{F} \equiv \frac{1}{4\pi} \int_{4\pi} d\vec{\Omega}' \bar{\nu} \sigma_f \quad (1f)$$

is the fission source operator and the distributed source is denoted with \mathcal{Q} . Here, σ_t is the total cross section, σ_s is the scattering cross section, σ_f the fission cross section with the fission spectrum χ and the average number of released neutrons $\bar{\nu}$, Y_l^p are the spherical harmonics and P_l the Legendre polynomials.

Equation (1a) is then formally solved for the angular flux as follows

$$\psi = -\frac{1}{\sigma_t} \vec{\Omega} \cdot \vec{\nabla} \psi + \frac{1}{\sigma_t} \mathcal{S}\psi + \frac{1}{\sigma_t} \mathcal{F}\psi + \frac{1}{\sigma_t} \mathcal{Q}. \quad (2)$$

Next we define the stabilization parameter τ as a function of a cell's optical thickness

$$\tau \equiv \begin{cases} \frac{1}{\sigma_t}, & \sigma_t h \geq \zeta \\ \frac{h}{\zeta}, & \sigma_t h < \zeta \end{cases} \quad (3)$$

with ζ the stabilization threshold, normally set to 0.5 as described in the reference [2]. We subtract and add $\tau\sigma_t\psi$ to ψ to obtain

$$\psi = (1 - \tau\sigma_t) \psi + \tau\sigma_t\psi. \quad (4)$$

Then we substitute Eq. (2) into the last term of the Eq. (4) to obtain

$$\psi = (1 - \tau \sigma_t) \psi + \tau \left(-\vec{\Omega} \cdot \vec{\nabla} \psi + \mathcal{S} \psi + \mathcal{F} \psi + \mathcal{Q} \right). \quad (5)$$

Substituting from Eq. (5) into the streaming term of the transport equation we obtain the SAAF τ equation for one energy group

$$\begin{aligned} -\vec{\Omega} \cdot \vec{\nabla} \left[\tau \vec{\Omega} \cdot \vec{\nabla} \psi \right] + \vec{\Omega} \cdot \vec{\nabla} [(1 - \sigma_t \tau) \psi] + \sigma_t \psi = \sum_{l=0}^L \sum_{p=-l}^l \frac{2l+1}{4\pi} Y_l^p(\vec{\Omega}_m) \sigma_l \phi_l^p \\ + \frac{1}{4\pi} \bar{\nu} \sigma_f \phi + \frac{q}{4\pi} - \vec{\Omega} \cdot \vec{\nabla} \left[\tau \sum_{l=0}^L \sum_{p=-l}^l \frac{2l+1}{4\pi} Y_l^p(\vec{\Omega}) \sigma_l \phi_l^p + \tau \frac{\bar{\nu} \sigma_f}{4\pi} \phi + \tau \frac{q}{4\pi} \right]. \end{aligned} \quad (6)$$

This equation is compatible with voids, however the system matrix is not symmetric anymore due to the first derivative. It will reduce to the first order transport equation in the case of $\tau = 0$. For $\zeta = 0$ the stabilization parameter Eq. (3) is $\tau = \frac{1}{\sigma_t}$ and Eq. (6) is equivalent to the standard SAAF form

$$\begin{aligned} -\vec{\Omega} \cdot \vec{\nabla} \left[\frac{1}{\sigma_t} \vec{\Omega} \cdot \vec{\nabla} \psi \right] + \sigma_t \psi = \sum_{l=0}^L \sum_{p=-l}^l \frac{2l+1}{4\pi} Y_l^p(\vec{\Omega}_m) \sigma_l \phi_l^p \\ + \frac{1}{4\pi} \bar{\nu} \sigma_f \phi + \frac{q}{4\pi} - \vec{\Omega} \cdot \vec{\nabla} \left[\frac{1}{\sigma_t} \sum_{l=0}^L \sum_{p=-l}^l \frac{2l+1}{4\pi} Y_l^p(\vec{\Omega}) \sigma_l \phi_l^p + \frac{1}{\sigma_t} \frac{\bar{\nu} \sigma_f}{4\pi} \phi + \frac{1}{\sigma_t} \frac{q}{4\pi} \right]. \end{aligned} \quad (7)$$

The weak form of the equation better defines the underlying physics than the classic partial-differential equation and can be converted to algebraic equations thus solved numerically with finite-dimensional function spaces. To derive the weak form we first multiply Eq. (6) by a test function ψ^* and integrate over the whole domain. Using integration by parts on all terms containing a derivative we obtain: find $\psi \in W_{\mathcal{D}}$ such that

$$\begin{aligned} \left(\tau \vec{\Omega} \cdot \vec{\nabla} \psi, \vec{\Omega} \cdot \vec{\nabla} \psi^* \right)_{\mathcal{D}} + \left((1 - \sigma_t \tau) \psi, \vec{\Omega} \cdot \vec{\nabla} \psi^* \right)_{\mathcal{D}} + \left(\sigma_t \psi, \psi^* \right)_{\mathcal{D}} + \left\langle \psi, \left(\vec{\Omega} \cdot \vec{n} \right) \psi^* \right\rangle_{\partial \mathcal{D}^+} \\ = \left(\sum_{l=0}^L \sum_{p=-l}^l \frac{2l+1}{4\pi} Y_l^p(\vec{\Omega}) \sigma_l \phi_l^p, \tau \vec{\Omega} \cdot \vec{\nabla} \psi^* + \psi^* \right)_{\mathcal{D}} + \left(\frac{\bar{\nu} \sigma_f}{4\pi} \phi, \tau \vec{\Omega} \cdot \vec{\nabla} \psi^* + \psi^* \right)_{\mathcal{D}} \\ + \left(\frac{q}{4\pi}, \tau \vec{\Omega} \cdot \vec{\nabla} \psi^* + \psi^* \right)_{\mathcal{D}} - \left\langle \psi^{\text{inc}}, \left(\vec{\Omega} \cdot \vec{n} \right) \psi^* \right\rangle_{\partial \mathcal{D}^-}, \end{aligned} \quad (8)$$

where the operator

$$(\cdot, \cdot)_{\mathcal{D}} \equiv \int_{\mathcal{D}} dV \quad (9)$$

is the standard spatial inner product and

$$\langle \cdot, \cdot \rangle_{\partial \mathcal{D}} \equiv \oint_{\partial \mathcal{D}} dA \quad (10)$$

is the corresponding surface integral over the boundary $\partial \mathcal{D}$. We further denote the incoming and outgoing boundary as

$$\partial \mathcal{D}^- = \left\{ \partial \mathcal{D} \mid \vec{\Omega} \cdot \vec{n} < 0 \right\} \quad (11a)$$

$$\partial \mathcal{D}^+ = \left\{ \partial \mathcal{D} \mid \vec{\Omega} \cdot \vec{n} > 0 \right\}. \quad (11b)$$

II.B. Weighted Least-Squares Method

The standard least-squares (LS) form of the transport equation [13]

$$(\mathcal{L} - \mathcal{S})^\dagger (\mathcal{L} - \mathcal{S}) \psi = (\mathcal{L} - \mathcal{S})^\dagger q \quad (12)$$

is not compatible with source iterations since the left hand side of the equation remains coupled in all directions. Here $(\mathcal{L} - \mathcal{S})^\dagger$ denotes the adjoint of the transport operator. The Least-Squares Equation derived by Hansen et al. [8] is a second order transport equation that is compatible with voids. In contrast to traditional least-squares forms this equation is also usable with source iterations with or without acceleration.

Consider the first order transport equation in operator form as shown in Eq. (1). Under the standard inner product

$$(\cdot, \cdot) \equiv \int_{\mathcal{D}} \int_{4\pi} \int_0^\infty dE d\Omega dV. \quad (13)$$

the adjoint of the streaming and collision operator Eq. (1b) is

$$\mathcal{L}^\dagger \equiv -\vec{\Omega} \cdot \vec{\nabla} + \sigma_t. \quad (14)$$

Multiplying Eq. (1a) with a weight function \mathcal{W} and the adjoint operator Eq. (14) gives the weighted least-squares equation compatible with source iteration

$$\mathcal{L}^\dagger \mathcal{W} \mathcal{L} \psi = \mathcal{L}^\dagger \mathcal{W} \mathcal{S} \psi + \mathcal{L}^\dagger \mathcal{W} \mathcal{F} \psi + \mathcal{L}^\dagger \mathcal{W} \mathcal{Q}. \quad (15)$$

Note that we only use the adjoint of the streaming and collision operator, and not the full adjoint to the transport equation. This gives us the ability to use source iterations and is the main difference relative to standard least-squares methods in Eq. (12). The left-hand side of this equation is self-adjoint and decouples for all directions, if the scattering and fission source are lagged with Source Iterations. The mono-energetic WLS equation can be written as

$$\begin{aligned} & -\vec{\Omega} \cdot \vec{\nabla} \left[w \vec{\Omega} \cdot \vec{\nabla} \psi \right] - \vec{\Omega} \cdot \psi \vec{\nabla} [w \sigma_t] + w \sigma_t^2 \psi \\ & = -\vec{\Omega} \cdot \vec{\nabla} \left[w \sum_{l=0}^L \sum_{p=-l}^l \frac{2l+1}{4\pi} Y_l^p(\vec{\Omega}) \sigma_l \phi_l^p + w \frac{\bar{\nu} \sigma_f}{4\pi} \phi + w \frac{q}{4\pi} \right] \\ & \quad + w \sigma_t \sum_{l=0}^L \sum_{p=-l}^l \frac{2l+1}{4\pi} Y_l^p(\vec{\Omega}) \sigma_l \phi_l^p + w \frac{\sigma_t \bar{\nu} \sigma_f}{4\pi} \phi + w \frac{q \sigma_t}{4\pi}. \end{aligned} \quad (16a)$$

where w denotes a weight function. The corresponding boundary conditions are

$$\psi(\vec{x}_b, \vec{\Omega}) = \psi^{\text{inc}}(\vec{x}_b, \vec{\Omega}), \quad \forall \vec{x}_b \in \partial \mathcal{D}, \quad \vec{\Omega} \cdot \vec{n} < 0 \quad (16b)$$

$$\vec{\Omega} \cdot \vec{\nabla} \psi(\vec{x}_b) + \sigma_t \psi(\vec{x}_b) = \mathcal{S} \psi(\vec{x}_b) + \mathcal{F} \psi(\vec{x}_b) + \mathcal{Q} \psi(\vec{x}_b), \quad \vec{\Omega} \cdot \vec{n} > 0. \quad (16c)$$

A rigorous property of transport solutions is causality. The definition of causality in this context is that the angular flux solution in a given direction is only influenced by upstream information. Given a point \vec{x} and a direction, $\vec{\Omega}$, the associated "upstream" points in an infinite medium are defined by

$$\vec{x}_{\text{upstream}} = \vec{x} - s \vec{\Omega} \quad \forall s \in \mathcal{R}^+, \quad (17a)$$

downstream is then accordingly

$$\vec{x}_{\text{downstream}} = \vec{x} + s \vec{\Omega} \quad \forall s \in \mathcal{R}^+. \quad (17b)$$

Second order forms however can be influenced by downstream information due to numerical errors. Problems with causality of these formulations occur at material interfaces separating optically thin and optically thick material regions. This is a coarse mesh problem that decreases with increasing refinement of the mesh. The

introduction of a weight function reduces this problem significantly [14]. Therefore we will use the weighted least-squares (WLS) equation with a weight function compatible with voids. The following weight function

$$w \equiv \frac{1}{\sigma_t} \quad (18)$$

improves the causality and makes our equations equivalent to the SAAF equation (Eq. (7)). Using Eq. (16a) with the weight function Eq. (18) the first derivative term becomes

$$\vec{\Omega} \cdot \psi \vec{\nabla} [w\sigma_t] = \vec{\Omega} \cdot \psi \vec{\nabla} [1] \equiv 0 \quad (19)$$

and the equation is equal to Eq. (7). However, the weight function Eq. (18) is not defined in voids. To compensate for this we redefine the weight function to

$$w \equiv \min \left(\frac{1}{\sigma_t}, w_{\max} \right), \quad (20)$$

where w_{\max} denotes a maximum value for the weight function. This definition will make the WLS equation well defined in voids and maintain the symmetric positive-definite properties of the resulting discretized matrix, that has to be inverted in the source iteration process. Therefore, the WLS equation is the same as the SAAF equation only for sufficiently large total cross section σ_t .

We derive the weak form by multiplying Eq. (16) with a test function ψ^* and integrate over the spatial domain \mathcal{D} , applying integration by parts to all terms containing a derivative. Given a trial space $W_{\mathcal{D}}$, consisting of continuous basis functions, the weak form is as follows: Find $\psi^* \in W_{\mathcal{D}}$ such that

$$\begin{aligned} & \left(w\vec{\Omega} \cdot \vec{\nabla} \psi, \vec{\Omega} \cdot \vec{\nabla} \psi^* + \sigma_t \psi^* \right)_{\mathcal{D}} + \left(w\sigma_t \psi, \vec{\Omega} \cdot \vec{\nabla} \psi^* + \sigma_t \psi^* \right)_{\mathcal{D}} \\ &= \left(w \sum_{l=0}^L \sum_{p=-l}^l \frac{2l+1}{4\pi} \sigma_l \phi_l^p Y_l^p(\vec{\Omega}), \vec{\Omega} \cdot \vec{\nabla} \psi^* + \sigma_t \psi^* \right)_{\mathcal{D}} + \left(w \frac{\nu \sigma_f}{4\pi} \phi + w \frac{q}{4\pi}, \vec{\Omega} \cdot \vec{\nabla} \psi^* + \sigma_t \psi^* \right)_{\mathcal{D}} \\ & \quad + \left\langle \vec{\Omega} \cdot \vec{\nabla} \psi + \sigma_t \psi, w \left(\vec{\Omega} \cdot \vec{n} \right) \psi^* \right\rangle_{\partial \mathcal{D}} \\ & \quad - \left\langle \sum_{l=0}^L \sum_{p=-l}^l \frac{2l+1}{4\pi} \sigma_l Y_l^p(\vec{\Omega}) \phi_l^p + \frac{\nu \sigma_f}{4\pi} \phi + \frac{q}{4\pi}, w \left(\vec{\Omega} \cdot \vec{n} \right) \psi^* \right\rangle_{\partial \mathcal{D}}. \quad (21) \end{aligned}$$

With the assumption that the first-order S_N transport equation is exactly satisfied on the boundary $\partial \mathcal{D}$, all of the boundary terms cancel, leading to the following:

$$\begin{aligned} & \left(w\vec{\Omega} \cdot \vec{\nabla} \psi, \vec{\Omega} \cdot \vec{\nabla} \psi^* + \sigma_t \psi^* \right)_{\mathcal{D}} + \left(w\sigma_t \psi, \vec{\Omega} \cdot \vec{\nabla} \psi^* + \sigma_t \psi^* \right)_{\mathcal{D}} \\ &= \left(w \sum_{l=0}^L \sum_{p=-l}^l \frac{2l+1}{4\pi} Y_l^p(\vec{\Omega}) \sigma_l \phi_l^p, \vec{\Omega} \cdot \vec{\nabla} \psi^* + \sigma_t \psi^* \right)_{\mathcal{D}} \\ & \quad + \left(w \frac{\nu \sigma_f}{4\pi} \phi + w \frac{q}{4\pi}, \vec{\Omega} \cdot \vec{\nabla} \psi^* + \sigma_t \psi^* \right)_{\mathcal{D}} \quad (22) \end{aligned}$$

An additional motivation for making this assumption is that it renders our Galerkin method for the second-order least-squares equation equivalent to the least-squares finite-element method for the first-order form of the S_N equations using the same trial space.

The natural boundary condition of Eq. (22) is a Dirichlet boundary condition. This is difficult to implement in numerical codes, since it is ambiguous at boundary corners and edges. We chose to use the optional weak boundary condition

$$\langle w f(\psi - \psi^{inc}), \psi^* \rangle_{\partial \mathcal{D}^-} \quad (23)$$

instead, where $\partial \mathcal{D}^-$ is the portion of the boundary for which $\vec{\Omega} \cdot \vec{n} < 0$.

We define

$$f \equiv \sigma_t \left| \vec{\Omega} \cdot \vec{n} \right| \quad (24)$$

based on the SAAF boundary condition [15]. However, the two SAAF boundary conditions are defined over the incoming and outgoing boundary respectively, while the optional WLS boundary conditions Eq. (23) are only defined on the incoming boundary. Nevertheless, with this boundary factor the WLS equation with optional boundary condition is still equivalent to the SAAF equation. To demonstrate this, we add the boundary term Eq. (23) to the left hand side of Eq. (22), insert the weight function given by Eq. (18), and integrate $(\vec{\Omega} \cdot \vec{\nabla} \psi, \psi^*)$ by parts to obtain

$$\begin{aligned} & \left(\frac{1}{\sigma_t} \vec{\Omega} \cdot \vec{\nabla} \psi, \vec{\Omega} \cdot \vec{\nabla} \psi^* \right)_{\mathcal{D}} + (\sigma_t \psi, \psi^*)_{\mathcal{D}} \\ & + \left\langle \psi, (\vec{\Omega} \cdot \vec{n}) \psi^* \right\rangle_{\partial \mathcal{D}} + \left\langle (\psi - \psi^{inc}), \left| \vec{\Omega} \cdot \vec{n} \right| \psi^* \right\rangle_{\partial \mathcal{D}^-} = 0. \end{aligned} \quad (25)$$

For simplification the source terms were set to zero. The boundary terms in Eq. (25) can now be manipulated as follows

$$\begin{aligned} & \left\langle \psi, (\vec{\Omega} \cdot \vec{n}) \psi^* \right\rangle_{\partial \mathcal{D}} + \left\langle (\psi - \psi^{inc}), \left| \vec{\Omega} \cdot \vec{n} \right| \psi^* \right\rangle_{\partial \mathcal{D}^-} \\ & = \left\langle \psi, (\vec{\Omega} \cdot \vec{n}) \psi^* \right\rangle_{\partial \mathcal{D}^+} + \left\langle \psi, (\vec{\Omega} \cdot \vec{n}) \psi^* \right\rangle_{\partial \mathcal{D}^-} \\ & \quad - \left\langle \psi, (\vec{\Omega} \cdot \vec{n}) \psi^* \right\rangle_{\partial \mathcal{D}^-} + \left\langle \psi^{inc}, (\vec{\Omega} \cdot \vec{n}) \psi^* \right\rangle_{\partial \mathcal{D}^-} \\ & = \left\langle \psi, (\vec{\Omega} \cdot \vec{n}) \psi^* \right\rangle_{\partial \mathcal{D}^+} + \left\langle \psi^{inc}, (\vec{\Omega} \cdot \vec{n}) \psi^* \right\rangle_{\partial \mathcal{D}^-}. \end{aligned} \quad (26)$$

This is the SAAF boundary condition as stated in Eq. (8).

For near void problems

$$f \equiv \max \left(\sigma_t, \frac{1}{h} \right) \left| \vec{\Omega} \cdot \vec{n} \right| \quad (27)$$

gives a more accurate and better conditioned version. Here h denotes a characteristic length constant of the boundary cell, we used the maximum distance between cell vertices, however this might not be a good choice for cells with a large aspect ratio. Thus even with optional boundary condition the WLS equation is equivalent to the SAAF equation, if and only if all σ_t are larger than the thresholds in the weight and boundary functions.

The resulting mono-energetic WLS equation used in this paper is defined as follows: Given a trial space $W_{\mathcal{D}}$, consisting of continuous basis functions, the weak form for a specific direction $m = 1 \dots M$ is as follows: Find $\psi^* \in W_{\mathcal{D}}$ such that

$$\begin{aligned} & \left(w \vec{\Omega} \cdot \vec{\nabla} \psi, \vec{\Omega} \cdot \vec{\nabla} \psi^* + \sigma_t \psi^* \right)_{\mathcal{D}} + \left(w \sigma_t \psi, \vec{\Omega} \cdot \vec{\nabla} \psi^* + \sigma_t \psi^* \right)_{\mathcal{D}} \\ & + \left\langle w f (\psi - \psi^{inc}), \psi^* \right\rangle_{\partial \mathcal{D}^-} = \left(w \sum_{l=0}^L \sum_{p=-l}^l \frac{2l+1}{4\pi} Y_l^p(\vec{\Omega}) \sigma_l \phi_l^p, \vec{\Omega} \cdot \vec{\nabla} \psi^* + \sigma_t \psi^* \right)_{\mathcal{D}} \\ & + \left(w \frac{\nu \sigma_f}{4\pi} \phi, \vec{\Omega} \cdot \vec{\nabla} \psi^* + \sigma_t \psi^* \right)_{\mathcal{D}} + \left(w \frac{q}{4\pi}, \vec{\Omega} \cdot \vec{\nabla} \psi^* + \sigma_t \psi^* \right)_{\mathcal{D}} \end{aligned} \quad (28)$$

with the weight function as described in Eq. (20) and the boundary functions as described in Eq. (27). Note that for $w = 1$ the WLS equation reduces to the unweighted LS scheme.

II.C. Nonlinear Diffusion Acceleration

We derive our low order diffusion equation from the first order transport equation as shown by Peterson [9]. This results in an independently differenced, but conservative form of the NDA, which enforces

conservation for the whole system. Integrating the mono-energetic transport equation over all angles gives us the zeroth moment equation

$$\vec{\nabla} \cdot \vec{J} + \sigma_t \phi = \sigma_s \phi + q. \quad (29)$$

To close Eq. (29), we consider the first moment equation

$$\sum_{m=1}^M \omega_m \vec{\Omega}_m \left(\vec{\Omega}_m \cdot \vec{\nabla} \psi_{m,g} \right) + \sigma_t \vec{J} = \sigma_1 \vec{J} \quad (30)$$

which gives the current

$$\vec{J} = -\frac{1}{\sigma_{tr}} \sum_{m=1}^M \omega_m \vec{\Omega}_m \left(\vec{\Omega}_m \cdot \vec{\nabla} \psi \right) \quad (31)$$

with the transport cross section

$$\sigma_{tr} \equiv \sigma_t - \sigma_1. \quad (32)$$

We use Eq. (31) to construct an additive correction to Fick's law by adding and subtracting $D \vec{\nabla} \phi$

$$\begin{aligned} \vec{J} &= -D \vec{\nabla} \phi + D \vec{\nabla} \phi - \frac{1}{\sigma_{tr}} \sum_{m=1}^M \omega_m \vec{\Omega}_m \vec{\Omega}_m \cdot \vec{\nabla} \psi \\ &= -D \vec{\nabla} \phi - \hat{\alpha} \phi \end{aligned} \quad (33)$$

with the drift vector

$$\hat{\alpha} \equiv \frac{1}{\phi} \left(\frac{1}{\sigma_{tr}} \sum_{m=1}^M \omega_m \vec{\Omega}_m \left(\vec{\Omega}_m \cdot \vec{\nabla} \psi \right) - D \vec{\nabla} \phi \right) \quad (34)$$

and the diffusion coefficient defined as

$$D \equiv \frac{1}{3\sigma_{tr}}. \quad (35)$$

Substituting Eq. (33) into Eq. (29) gives the NDA drift-diffusion equation

$$-\vec{\nabla} \cdot [D \vec{\nabla} \phi] - \vec{\nabla} \cdot [\hat{\alpha} \phi] + \sigma_a \phi = q. \quad (36)$$

Multiplying Eq. (29) by a test function ϕ^* and integrating over the domain gives the corresponding weak form

$$\left(\vec{\nabla} \cdot \vec{J}, \phi^* \right)_{\mathcal{D}} + (\sigma_a \phi, \phi^*)_{\mathcal{D}} = (q, \phi^*)_{\mathcal{D}}. \quad (37)$$

Applying integration by parts on the current term and substituting Eq. (33) gives

$$-\left(D \vec{\nabla} \phi, \vec{\nabla} \phi^* \right)_{\mathcal{D}} - \left(\hat{\alpha} \phi, \vec{\nabla} \phi^* \right)_{\mathcal{D}} + \left\langle \vec{n} \cdot \vec{J}, \phi^* \right\rangle_{\partial \mathcal{D}} + (\sigma_a \phi, \phi^*)_{\mathcal{D}} = (q, \phi^*)_{\mathcal{D}}. \quad (38)$$

The boundary term $\left\langle \vec{n} \cdot \vec{J}, \phi^* \right\rangle_{\partial \mathcal{D}}$ still needs to be evaluated. While the reflective boundary condition is natural to the diffusion equation, the vacuum condition is more challenging. Using the partial currents we can define

$$\begin{aligned} \left\langle \vec{n} \cdot \vec{J}, \phi^* \right\rangle_{\partial \mathcal{D}} &= \left\langle J^{\text{out}} - J^{\text{in}}, \phi^* \right\rangle_{\partial \mathcal{D}} \\ &= \left\langle \frac{1}{4} \kappa \phi - J^{\text{in}}, \phi^* \right\rangle_{\partial \mathcal{D}} \end{aligned} \quad (39)$$

with the vacuum boundary coefficient as

$$\begin{aligned} \kappa &\equiv 4 \frac{J^{\text{out}}}{\phi} \\ &= \frac{4}{\phi} \sum_{\vec{n} \cdot \vec{\Omega}_m > 0} \omega_m \left(\vec{n} \cdot \vec{\Omega}_m \right) \psi \end{aligned} \quad (40)$$

and substitute this into the boundary term. Note that we changed the vacuum boundary coefficient from the one described in [9] to Eq. (40) to be consistent with the SAAF τ implementation in Rattlesnake [2].

For a given iteration k the NDA scheme is defined as follows:

1. Solve the WLS transport equation

$$\begin{aligned} & \left(\mathbf{w} \vec{\Omega} \cdot \vec{\nabla} \psi^{k+\frac{1}{2}} + \mathbf{w} \sigma_{\text{t}} \psi^{k+\frac{1}{2}}, \vec{\Omega} \cdot \vec{\nabla} \psi^* + \sigma_{\text{t}} \psi^* \right)_{\mathcal{D}} \\ & \quad + \left\langle \mathbf{w} f \left(\psi^{k+\frac{1}{2}} - \psi^{\text{inc}} \right), \psi^* \right\rangle_{\partial \mathcal{D}^-} \\ & = \left(\mathbf{w} \sum_{l=0}^L \sum_{p=-l}^l \frac{2l+1}{4\pi} Y_l^p \sigma_l \phi_l^{p,k}, \vec{\Omega} \cdot \vec{\nabla} \psi^* + \sigma_{\text{t}} \psi^* \right)_{\mathcal{D}} \\ & \quad + \left(\mathbf{w} \frac{1}{4\pi} \nu \sigma_{\text{f}} \phi^k + \mathbf{w} \frac{1}{4\pi} q, \vec{\Omega} \cdot \vec{\nabla} \psi^* + \sigma_{\text{t}} \psi^* \right)_{\mathcal{D}}, m = 1 \dots M \end{aligned} \quad (41a)$$

2. Calculate the correction terms for the diffusion equation

$$\kappa^{k+\frac{1}{2}} = \frac{4}{\phi} \sum_{\vec{n} \cdot \vec{\Omega}_m > 0} \omega_m \left(\vec{n} \cdot \vec{\Omega}_m \right) \psi^{k+\frac{1}{2}} \quad (41b)$$

$$\hat{\alpha}^{k+\frac{1}{2}} = \frac{1}{\phi^{k+\frac{1}{2}}} \left(\frac{1}{\sigma_{\text{tr}}} \sum_{m=1}^M \omega_m \vec{\Omega}_m \left(\vec{\Omega}_m \cdot \vec{\nabla} \psi_m^{k+\frac{1}{2}} \right) - \text{D} \vec{\nabla} \phi^{k+\frac{1}{2}} \right) \quad (41c)$$

3. Solve the diffusion equation

$$\begin{aligned} & - \left(\text{D} \vec{\nabla} \phi^{k+1}, \vec{\nabla} \phi^* \right)_{\mathcal{D}} - \left(\hat{\alpha}^{k+\frac{1}{2}} \phi^{k+1}, \vec{\nabla} \phi^* \right)_{\mathcal{D}} \\ & \quad + \left\langle \frac{\kappa^{k+\frac{1}{2}}}{4} \phi^{k+1} - J^{\text{in}}, \phi^* \right\rangle_{\partial \mathcal{D}} + \left(\sigma_{\text{a}} \phi^{k+1}, \phi^* \right)_{\mathcal{D}} = \left(q, \phi^* \right)_{\mathcal{D}} \end{aligned} \quad (41d)$$

4. Check convergence and update the scattering source

$$\frac{\|\phi^{l+1} - \phi^l\|}{\phi^l} \leq \tau \quad (41e)$$

The iteration scheme for the NDA starts with a low order solve of Eq. (41d) assuming $\hat{\alpha}^{\frac{1}{2}} = 0$ and $\kappa^{\frac{1}{2}} = 1$. The scalar flux is transferred to the high order system and used for the scattering and fission source. The new angular flux is obtained and the drift vector and boundary coefficient calculated. These are then used for the next low order diffusion solve. This iteration continues until convergence of the low order and high order solutions.

The derivation of the multi-group equations is similar. The only thing to be considered are the cross-group scattering terms in the drift vector

$$\hat{\alpha}_g^{k+\frac{1}{2}} \equiv \frac{1}{\phi_g^{k+\frac{1}{2}}} \left(\frac{1}{\sigma_{\text{tr},g}} \sum_{m=1}^M \omega_m \vec{\Omega} \left(\vec{\Omega} \cdot \vec{\nabla} \psi_{m,g}^{k+\frac{1}{2}} \right) - \frac{1}{\sigma_{\text{tr},g}} \sum_{\substack{g'=1 \\ g' \neq g}}^G \sigma_{1,g' \rightarrow g} \vec{J}_{g'}^{k+\frac{1}{2}} - \text{D}_g \vec{\nabla} \phi_g^{k+\frac{1}{2}} \right). \quad (42)$$

III. NUMERICAL RESULTS

III.A. Implementation in Rattlesnake

The high-order low-order system is represented by two sets of equation systems in Rattlesnake. The low-order diffusion equation is solved with the PJFNK solver [11] preconditioned with Hypre BoomerAMG [16]. BoomerAMG is not specifically designed for the non-symmetric Jacobian of this system. Currently there is a study in progress to replace it with an AMG solver for anisotropic diffusion [17, 18], which is better suited for non-axis aligned problems. Nevertheless, for now BoomerAMG is an effective preconditioner. Before the actual solve Rattlesnake performs several free power iterations. The power iterations ensure that the initial guess for the Newton solve is close to the largest eigenvalue. All consecutive solves use Picard iterations. Each Picard iterations consists of the steps corresponding to Eq. (41). First the low-order equation is solved using a nonlinear eigenvalue solver [19] to obtain an initial guess for the scalar flux. The scalar flux is transferred to the high-order system. The left hand side of the transport equation, the streaming and collision part, is inverted. Finally, the drift vector and boundary coefficients are updated using the angular fluxes. The implementation of the correction terms and low-order equation is set up to allow the reuse of code for WLS and SAAF τ implementations.

Given a specific mesh and an angular quadrature, the left hand side operator of both WLS and SAAF τ equation are fixed, and therefore the matrix can be assembled during the initial setup. Since the low order and high-order system use the same mesh, the spatial quadrature points are identical. All coefficients and drift vectors are only evaluated on the quadrature points and then transferred to the low-order system. The low-order system uses the same code for both high-order schemes. Code duplications were also avoided for the boundary coefficient and transfer routines, only the evaluation of the drift vector is different between WLS and SAAF.

All one-dimensional results were generated using a simpler Python research code. This code allowed better control and easier modifications. The numerical solver was the SciPy sparse linear algebra solver.

III.B. Comparison of weighted and unweighted LS

To test the effect of the weighting on the LS equation, consider a one dimensional problem with two material regions. The left region contains a weak absorber ($\sigma_{t,1} = \sigma_{a,1} = 0.1 \frac{1}{\text{cm}}$), while the right region has a strong absorber ($\sigma_{t,2} = \sigma_{a,2} = 10 \frac{1}{\text{cm}}$). Each region is 1 cm thick and discretized with 8 cell. The problem is surrounded by vacuum. A constant source of $q = 1 \frac{n}{\text{s-cm}}$ is added in both regions. We compared the unweighted LS to the weighted LS and the SAAF and SAAF τ formulation in Rattlesnake. The SAAF τ scheme used $\zeta = 0.5$, and all calculations employed a S_8 Gauss quadrature. Note that w_{max} is not needed, since the problem does not contain a void.

The purpose of these test problems were to evaluate the pure LS and WLS equations. No NDA was used, which would enforce conservation, even though acceleration is unnecessary in a purely absorbing geometry. Figure 1 shows the results for the scalar flux. The LS result in the left half of the problem was strongly influenced by the thick material in the right half. The introduction of the weight function for the WLS ameliorated this problem. The results still show a decrease towards the thick region, however it is significantly less compared to the unweighted LS. The reason, that the WLS scheme gives a different results than the SAAF is the boundary condition, Eq. (27). The cell size is too large, so the void guard is triggered. If we use Eq. (24) instead, we obtain the same result as the SAAF calculations. The SAAF τ scheme was closest to the reference solution, but it had a strong decrease in the cell next to the material interface and oscillations left of that cell. We note the large difference between the SAAF method and the SAAF τ method, even though no voids are present. With the default setting $\zeta = 0.5$, the void stabilization is already activated for most reactor physics problems and hence influences the results.

The results for the angular fluxes in Fig. 2 showed that the error for the WLS scheme is strongly dependent on the angle μ . For more perpendicular directions the error was larger (Fig. 2) than for μ closer to one. Note that the angular flux can be negative, because the WLS scheme is not strictly non-negative since the matrix is not monotone.

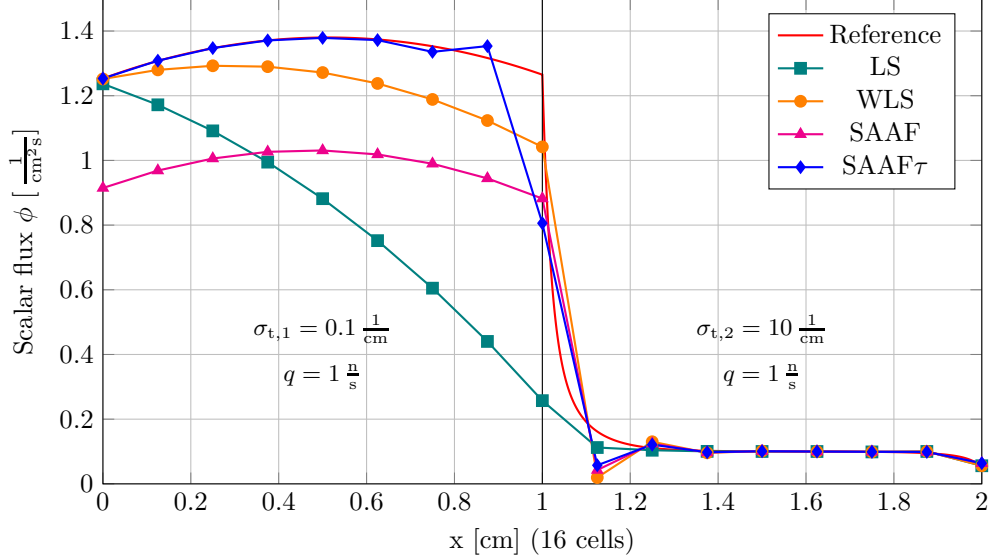


Fig. 1. Comparison of the scalar flux results for the two absorber problem with a source using the second order transport schemes.

III.C. Weight function limit in voids

As stated in Section II.B, the weight function must be limited to be defined in void regions. We further studied the influence of the maximal weight w_{\max} of the WLS implementation in a problem with void to obtain an estimate of w_{\max} necessary for good accuracy. If w_{\max} is too small, the accuracy will be low, however, the larger w_{\max} gets, the more the discretization matrix becomes ill-conditioned.

The test problem is a two region slab with a void ($\sigma_{t,1} = 0 \frac{1}{\text{cm}}$) on the left side and a strong absorber ($\sigma_{t,2} = 10 \frac{1}{\text{cm}}$) on the right side. Two subcases with an isotropic flux of $\phi^{\text{inc}} = 1 \frac{1}{\text{cm}^2\text{s}}$ on the left or the right boundary respectively demonstrate the directionality of the problem. For all calculations a S_8 quadrature were used.

Figure 3 shows the scalar flux results for the left inflow case. The increase of the maximal weight improved the slope of the scalar flux significantly in the void region. However, the increase resulted in a stronger dip after the material interface. The reduction in the relative error

$$e \equiv \frac{\|\phi(x) - \phi_{\text{exact}}(x)\|_{L_2}}{\|\phi_{\text{exact}}(x)\|_{L_2}} \quad (43)$$

with increasing w_{\max} is shown in Fig. 4. The reference solution is a spatially analytic solution using the same angular quadrature. The convergence is shown for the error of the whole domain (void and material region) and for the void region separately. The ratio between these two errors is a good indicator for the effectiveness of the weighting, since w_{\max} strongly influences the void region, but has almost no effect in the material region except for the first few nodes. We can see that for the left inflow case the error in the void converged with first order for increasing w_{\max} . For $w_{\max} < 10 \text{ cm}$ the error in the void region dominated the error for the whole problem, however for larger w_{\max} the error in the material region dominated and hence no further error reduction can be seen. From this we concluded that a w_{\max} in the range between 100 cm and 1000 cm is sufficient for this problem. For the right inflow problem Fig. 5 shows that w_{\max} had no effect on the error in both the whole domain and void region. This clearly demonstrates the directionality of the causality problem.

The values for w_{\max} are problem dependent. In the following section, we evaluate the influence of several parameters on the required w_{\max} . Again we will look at the ratio of the error in the void region to the total error as a function of w_{\max} . The first parameter we looked at is the mesh size. We ran a study on the effects of mesh refinement on the optimal limit of the weight function. Our results showed that the optimal weight limit is almost independent from the mesh refinement as shown in Fig. 6. In the figure, the solid lines

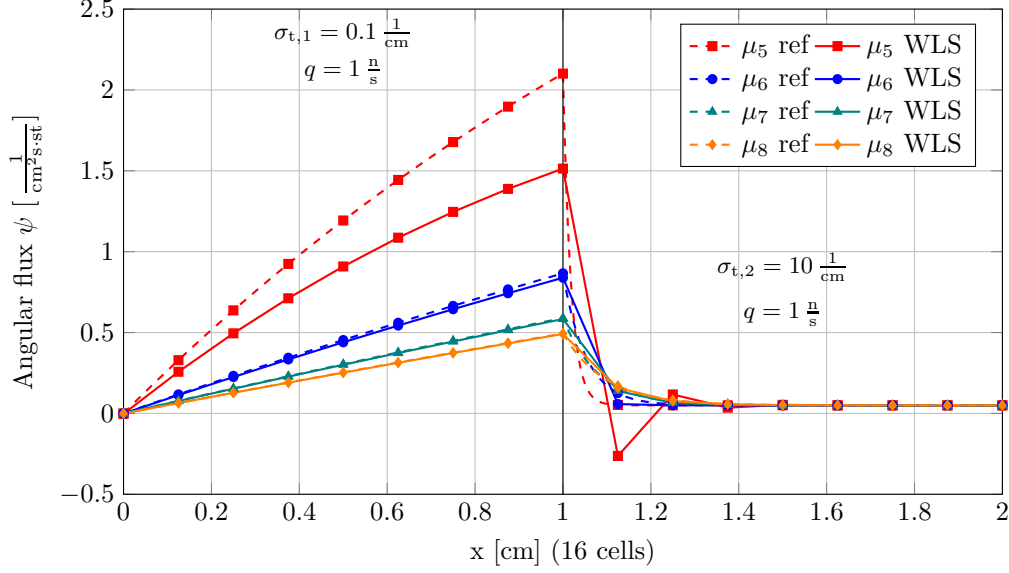


Fig. 2. Comparison of the angular flux for positive angles between the WLS (solid line) and the reference solution (dashed) depending on the angle μ ($0 < \mu_5 < \mu_6 < \mu_7 < \mu_8 < 1$).

TABLE I

w_{\max} for which the error in the vacuum is 10% of the total error based on the parameters L_1 , L_2 and $\sigma_{t,2}$.

Value of parameter $L_1[\text{cm}], L_2[\text{cm}], \sigma_{t,2} [\text{cm}^{-1}]$	$w_{\max}(L_1)$ [cm]	$w_{\max}(L_2)$ [cm]	$w_{\max}(\sigma_{t,2})$ [cm]
1	48.4	48.4	48.4
2	96.8	64.9	64.9
5	242.1	98.4	98.4
10	484.1	136.8	136.8

show the error for the whole problem, the dashed lines the error for the vacuum part of the problem. For all mesh sizes we observed the same behavior, that at approximately $w_{\max} = 100 \text{ cm}$ the error in the void is almost a magnitude lower than the total error and hence its contribution to the total error is negligible and other error sources dominate. This indicates that the mesh size has no significant effect on the required w_{\max} .

The second set of calculations addresses the influence of geometric parameters on the optimal w_{\max} . The base problem used for these calculations is similar to the previous problem. It is a two region problem with void on the left ($\sigma_{t,1} = \sigma_{a,1} = 0 \frac{1}{\text{cm}}, L_1 = 1 \text{ cm}$) and an absorber on the right with $\sigma_{t,2} = \sigma_{a,2} = 1 \frac{1}{\text{cm}}$ and a width of $L_2 = 1 \text{ cm}$. By changing each of the parameters L_1 , L_2 and $\sigma_{t,2}$ separately and locking at the ratio of the error in the void region to the total error we can study their sensitivity on the required maximal weight. Every calculation used 1024 cells to provide a good spatial resolution. Figures 7 to 9 show the results for this parameter study. The red line in every plot is the default configuration without changed parameters as described above. A ratio close to one shows that the error in the void region is dominant, while a small ratio indicates a small influence of the void error and that other sources of error dominate.

Figure 7 shows that the width of the vacuum region has the strongest influence on the needed w_{\max} , while the width of the material region and the corresponding cross section have both a smaller influence (Figs. 8 and 9). This can be easier seen in Table I, which shows the w_{\max} for which the error in the vacuum regions is only 0.1 of the total error. While an increase in L_1 of a factor of ten results in an increase of the required weight limit of the same factor, this factor is only approximately 2.8 for both L_2 and $\sigma_{t,2}$.

We showed already, that the error of the angular flux is strongly dependent on the angle (Fig. 2). Given

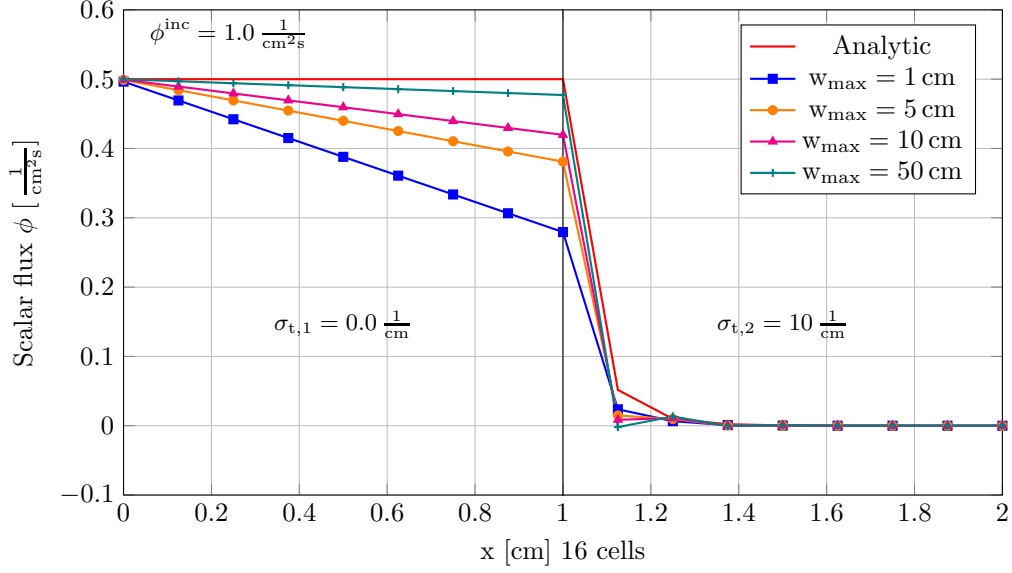


Fig. 3. Scalar fluxes using the WLS transport scheme for different weight function limit w_{\max} for the two region void problem with left inflow.

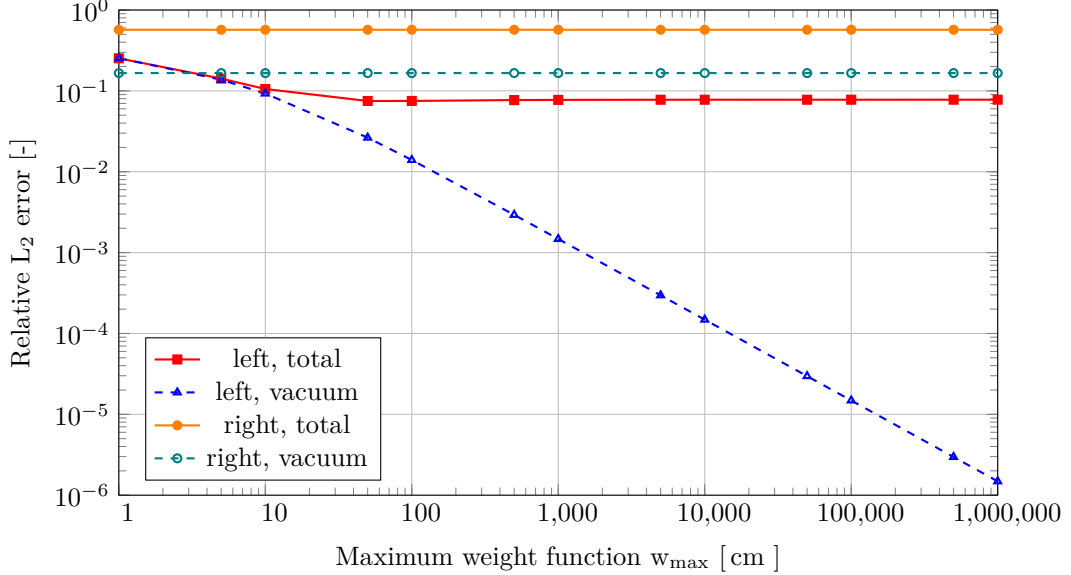


Fig. 4. Error convergence with increasing weight function limit w_{\max} for the two region void problem with left or right inflow for the total error and the error in the vacuum region separately.

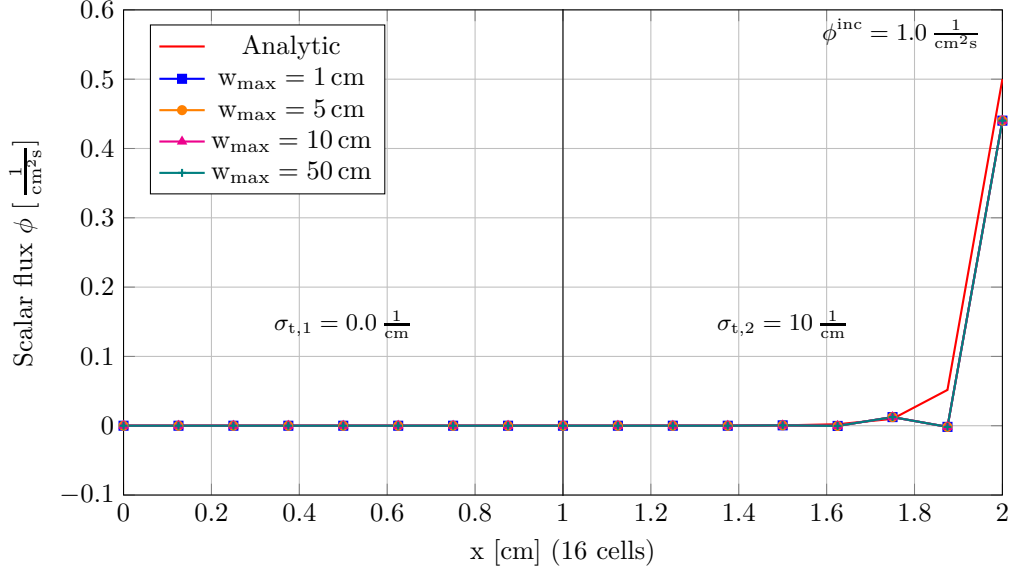


Fig. 5. WLS scalar fluxes results for different weight function limits w_{\max} for the two region void problem with right inflow.

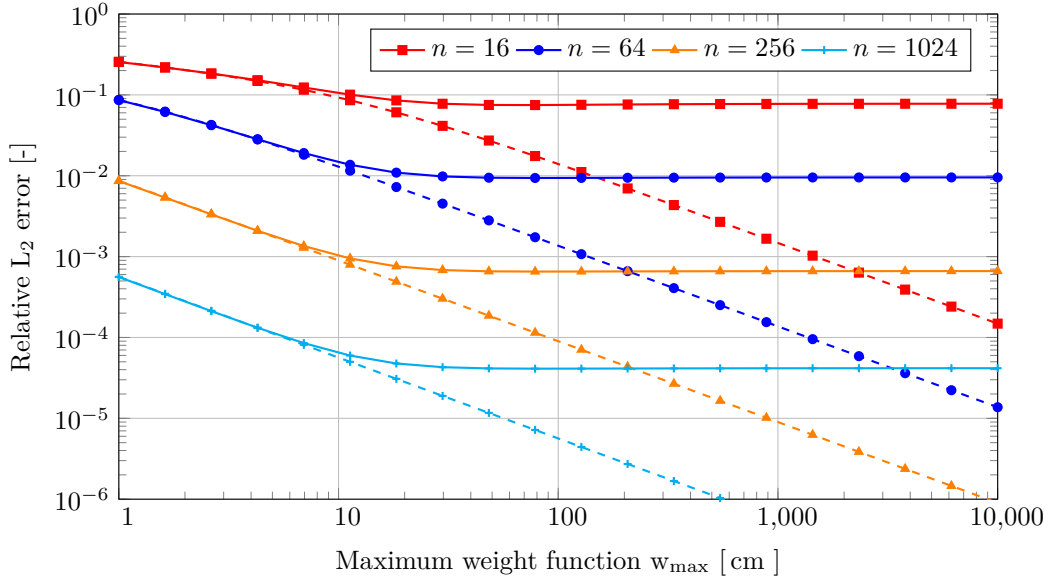


Fig. 6. The error convergence with increasing weight function limit w_{\max} using different mesh sizes n for the two region void problem with left inflow (solid line for the total error, dashed for the error in the vacuum region).

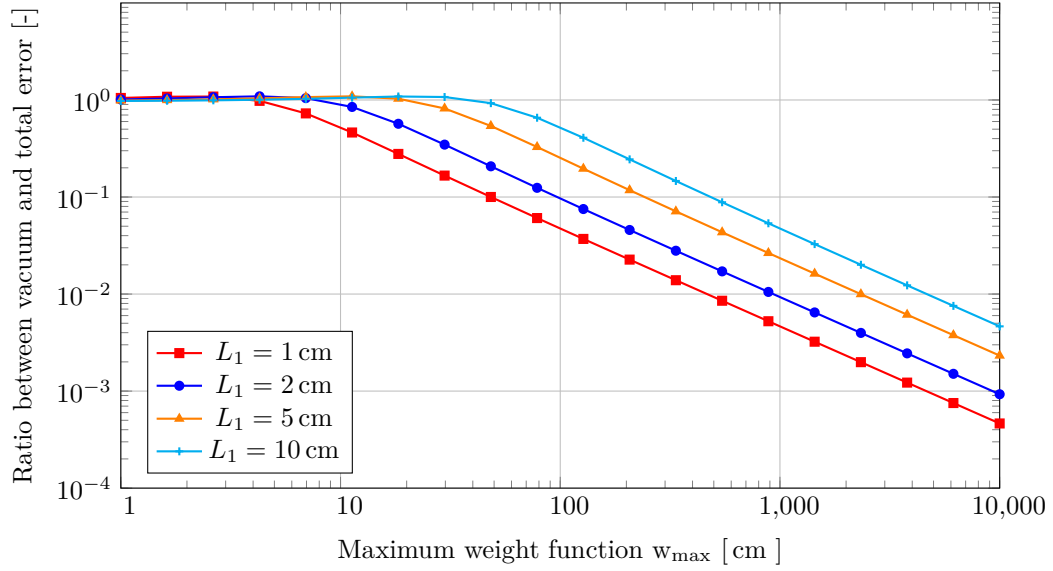


Fig. 7. Ratio of the error in the vacuum region to the total error as a function of w_{max} with different widths L_1 of the vacuum region for the two region problem with $n = 1024$, $\sigma_{t,2} = 1 \frac{1}{\text{cm}}$ and $L_2 = 1 \text{ cm}$

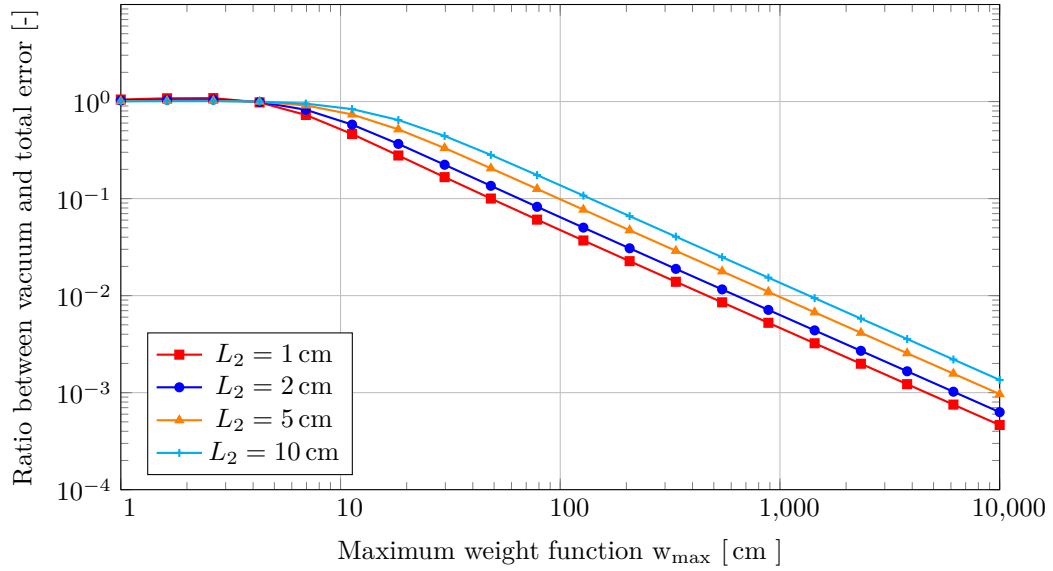


Fig. 8. Ratio of the error in the vacuum region to the total error as a function of w_{max} with different widths L_2 of the material region for the two region problem with $n = 1024$, $\sigma_{t,2} = 1 \frac{1}{\text{cm}}$ and $L_1 = 1 \text{ cm}$

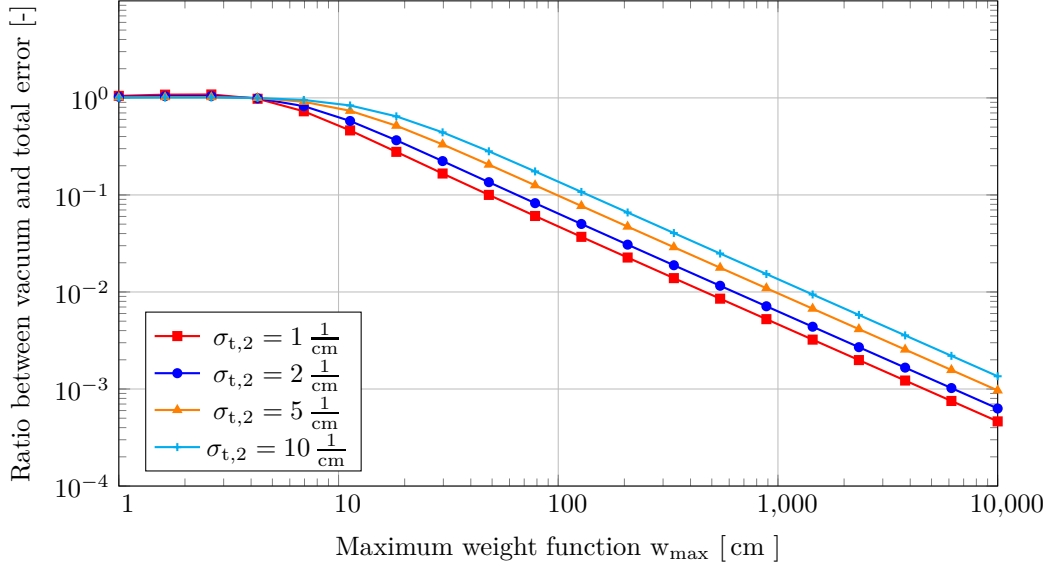


Fig. 9. Ratio of the error in the vacuum region to the total error as a function of w_{max} with different $\sigma_{t,2}$ of the material region for the two region problem with $n = 1024$, $L_1 = 1$ cm and $L_2 = 1$ cm

TABLE II

w_{max} with an angular dependent weight function (Eq. (44)) for which the error in the vacuum is 10% of the total error based on the parameters L_1 , L_2 and $\sigma_{t,2}$.

Value of parameter L_1 [cm], L_2 [cm], $\sigma_{t,2}$ [cm ⁻¹]	$w_{max}(L_1)$ [cm]	$w_{max}(L_2)$ [cm]	$w_{max}(\sigma_{t,2})$ [cm]
1	9.7	9.7	9.7
2	19.4	13.1	13.1
5	48.6	19.8	19.8
10	97.2	27.6	27.6

the fact, that the width of the void region is an important factor on how high the limit of the weight function must be and that the track length through the void is proportional to μ^{-1} , we can modify the limit to address the angular issue. Changing the weight function to

$$w_m \equiv \min \left(\frac{1}{\sigma_t}, \frac{w_{max}}{\mu_m} \right) \quad (44)$$

will change the w_{max} for a ratio of 10% between vacuum error and total error to the values shown in Table II. This is a decrease by a factor of five compared to the previous values. This result is only meaningful in one-dimensional problems, the implementation in more dimensions is not clear.

III.D. C5G7 benchmark

The C5G7 MOX benchmark problem is a challenging test for modern deterministic transport codes. We focused on the two dimensional version of the benchmark, which already requires large amounts of computational resources. The twenty sets of results that were initially submitted to the benchmark committee can be found in a special issue of Progress in Nuclear Energy [20]. More recent calculations of the benchmark with a spatial and angular convergence study were presented by McGraw [21] using PDT and Wang [22] using Rattlesnake. These calculations were used as a reference solution to benchmark and validate the WLS implementation in Rattlesnake.

Fig. 10. Zone layout of the C5G7 benchmark geometry. Reprinted from Wang et. al. [22].

TABLE III

Comparison of the eigenvalue error and the pin power errors for the transport and NDA schemes with 4 polar and 32 azimuthal angles. Column PP1 shows the relative error for the maximal pin power and PP2 the error for the minimal power.

Scheme	k_{eff} [pcm]	AVG [%]	RMS [%]	MRE [%]	MAX [%]	PP1 [%]	PP2 [%]
LS	15880.916	8.354	0.336	11.640	30.847	12.345	4.255
WLS	87.741	0.400	0.016	0.539	1.661	0.608	1.123
SAAF	87.741	0.400	0.016	0.539	1.661	0.608	1.123
SAAF τ	52.115	0.249	0.010	0.350	1.178	0.433	0.195
NDA LS	52.682	0.380	0.015	0.488	1.613	0.444	1.662
NDA WLS	87.740	0.400	0.016	0.539	1.661	0.608	1.123
NDA SAAF	87.741	0.400	0.016	0.539	1.661	0.608	1.123
NDA SAAF τ	52.115	0.249	0.010	0.350	1.178	0.433	0.195

The mesh is generated using the 2D mesh generator Triangle [23] with a geometry file which is created by a Rattlesnake mesh generator. The quality of the mesh ensures that no triangle has an interior angle less than 20 degrees. In order to limit the number of elements in the mesh, the surrounding reflector region is divided into three separate regions as shown in Fig. 10, employing a coarser mesh far away from the fuel region, while the same maximum triangle area is applied to all fuel assemblies. The mesh conserves the volume of each fuel pin and hence the mass of fissile material. More details about the mesh can be found in the original paper [22].

We performed calculations to compare the LS, WLS, SAAF and SAAF τ transport and NDA schemes. These calculations were performed with Gauss-Chebyshev quadrature with 4 polar and 32 azimuthal angles. A angular refinement study showed that these settings were sufficient to minimize the angular error. For the transport solution a relative tolerance to the initial solution of 10^{-8} was used. The NDA calculations used as error tolerance the difference between two consecutive scalar flux solutions with a threshold of 10^{-8} , and a high order relative tolerance of 10^{-4} . These tolerances were used for all following calculations.

The results are shown in Table III. The non-conservative LS transport formulation showed large deviations in all errors. This demonstrates how important the use of a conservative scheme for criticality calculations is. The WLS transport solution was exactly the same as the SAAF solution, as expected for a problem without voids. The best result for all errors gave the SAAF τ scheme with $\zeta = 0.5$, even though no voids are present in the benchmark.

The results for the NDA schemes are shown in the second part of Table III. The use of the conservative NDA with the non-conservative LS scheme showed that the NDA ensures conservation. The NDA LS result was within a reasonable range of error, with the error in the eigenvalue one of the lowest for all schemes. The errors in the pin power were also much lower compared to the LS transport solution, and of the same magnitude as the results of the NDA using SAAF and WLS. The NDA SAAF τ scheme gave the smallest errors for pin powers. Again SAAF and WLS, this time with NDA, gave the same results. The NDA results for WLS, SAAF and SAAF τ were consistent with the corresponding transport solves.

The comparison of the runtime for all schemes and the number of NDA iterations are shown in Table IV. All calculations were performed on 2 nodes of INL's HPC cluster Falcon [24] with 36 cores per node. The calculation times for pure transport were much longer than for the NDA schemes.

IV. CONCLUSIONS

We derived a weighted LS transport equation and showed that we can make this equation equivalent to the SAAF equation by using a particular weight function. However, this weight function is not compatible

TABLE IV

Comparison of the pure transport and NDA calculation time and the number of NDA iterations for the original C5G7 benchmark.

Scheme	Transport Time [h]	NDA	
		Time [h]	Iterations [-]
LS	5.15	0.29	16
WLS	4.47	0.29	15
SAAF	4.25	0.28	15
SAAF τ	4.79	0.23	15

with voids. So to be able to handle voids, the weight function and the boundary conditions were modified. With these modifications, the SAAF and weighted least-squares equations are equal only for sufficiently large cross sections. The primary advantage of a weight function is an improvement in causality, i.e., a reduction in the extent to which downstream quantities affect the transport solution. The discretization of the WLS scheme is, in contrast to the SAAF τ scheme, symmetric positive definite in problems with voids. This, as mentioned earlier, allows the use of more memory efficient linear solvers with faster convergence.

We analyzed limiting of the weight function to obtain best results for certain test problems. Limiting is required not only because the default weight function becomes unbounded in a void, but also because the coefficient matrix becomes increasingly ill-conditioned as the variation of the weight function increases. Numerical evidence indicates that the weight function limit is a function of the geometry and strongly dependent on the width of the void region, while less impacted by the optical thickness of the surrounding regions.

The weighted least-squares method and the corresponding NDA scheme were fully implemented in Rattlesnake. The C5G7 benchmark was used to test the NDA scheme on a more challenging 2-D problem. The comparison between NDA WLS, NDA SAAF τ , and reference PDT calculations showed that the WLD NDA results are sometimes less accurate than the NDA SAAF τ results, but nonetheless comparable. A major advantage of the NDA WLS scheme relative to the NDA SAAF τ scheme is that the NDA WLS high-order equations are symmetric positive-definite. Thus the NDA WLS scheme can use the conjugate-gradient method to solve the high-order equation, which requires the storage of only three solutions vectors. More general Krylov solvers such as GMRES, can require an arbitrary number of solutions vectors or a restart with degraded convergence properties. This gives the NDA WLS scheme an enormous advantage regarding memory requirements.

Based on this work, we intend to continue testing the NDA WLS scheme on more complicated problems with and without voids.

V. ACKNOWLEDGMENTS

This material is based upon work supported by the Department of Energy, Battelle Energy Alliance, LLC, under Award Number DE-AC07-05ID14517.

REFERENCES

- [1] Y. WANG, S. SCHUNERT, M. DEHART, R. MARTINEAU, and W. ZHENG, “Hybrid with Lagrange Multiplier and Upwinding for the Multiscale Transport Capability in Rattlesnake,” *Progress in Nuclear Energy* (2017); 10.1016/j.pnucene.2017.03.020.
- [2] Y. WANG, H. ZHANG, and R. C. MARTINEAU, “Diffusion Acceleration Schemes for Self-Adjoint Angular Flux Formulation with a Void Treatment,” *Nuclear Science and Engineering*, **176**, 2, 201 (2014).
- [3] D. GASTON, C. NEWMAN, G. HANSEN, and D. LEBRUN-GRANDIE, “MOOSE: A Parallel Computational Framework for Coupled Systems of Nonlinear Equations,” *Nuclear Engineering and Design*, **239**, 10, 1768 (2009).

- [4] C. J. GESH, “Finite Element Methods for Second Order Forms of the Transport Equation,” PhD Thesis, Texas A&M University (1999).
- [5] Y. SAAD, *Iterative Methods for Sparse Linear Systems, Second Edition*, Society for Industrial and Applied Mathematics, Philadelphia (2003).
- [6] R. T. ACKROYD, J. G. ISSA, and N. S. RIYAIT, “Treatment of Voids in Finite Element Transport Methods,” *Progress in Nuclear Energy*, vol. 18 of *Progress in Nuclear Energy (UK)*, 85–9 (18); 10.1016/0149-1970(86)90015-6.
- [7] J. E. MOREL and J. M. MCGHEE, “A Self-Adjoint Angular Flux Equation,” *Nuclear Science and Engineering*, **132**, 3, 312 (1999).
- [8] J. HANSEN, J. R. PETERSON, J. E. MOREL, J. C. RAGUSA, and Y. WANG, “A Least-Squares Transport Equation Compatible with Voids,” *Journal of Computational and Theoretical Transport*, **43**, 1-7, 374 (2014).
- [9] J. R. PETERSON, H. HAMMER, J. E. MOREL, J. C. RAGUSA, and Y. WANG, “Conservative Nonlinear Diffusion Acceleration Applied to the Unweighted Least-Squares Transport Equation in MOOSE,” *Mathematics and Computations, Supercomputing in Nuclear Applications and Monte Carlo International Conference, M and C+SNA+MC 2015, April 19, 2015 - April 23, 2015*, vol. 1, 636–648, American Nuclear Society (2015).
- [10] M. L. ADAMS and E. W. LARSEN, “Fast Iterative Methods for Discrete-Ordinates Particle Transport Calculations,” *Progress in Nuclear Energy*, **40**, 1, 3 (2002); 10.1016/S0149-1970(01)00023-3.
- [11] H. PARK, D. A. KNOLL, and C. K. NEWMAN, “Nonlinear Acceleration of Transport Criticality Problems,” *Nuclear Science and Engineering*, **172**, 1, 52 (2012).
- [12] H. HAMMER, J. E. MOREL, and Y. WANG, “Nonlinear Diffusion Acceleration of the Least-Squares Transport Equation in Geometries with Voids,” *Nuclear Science and Engineering* (2018); 10.1080/00295639.2018.1542865.
- [13] C. DRUMM, W. FAN, A. BIELEN, and J. CHENHALL, “Least-Squares Finite-Element Algorithms in the SCEPTRE Radiation Transport Code,” *International Conference on Mathematics and Computational Methods Applied to Nuclear Science and Engineering (M&C 2011)*, American Nuclear Society, Rio de Janeiro, RJ, Brazil (2011).
- [14] W. ZHENG, “Least-Squares and Other Residual Based Techniques for Radiation Transport Calculations,” Dissertation, Texas A&M University, College Station, TX (2016).
- [15] V. M. LABOURE, Y. WANG, and M. D. DEHART, “Least-Squares PN Formulation of the Transport Equation Using Self-Adjoint-Angular-Flux Consistent Boundary Conditions,” *Physics of Reactors 2016: Unifying Theory and Experiments in the 21st Century, PHYSOR 2016*, vol. 5, 3376–3385, American Nuclear Society (2016).
- [16] V. E. HENSON and U. M. YANG, “BoomerAMG: A Parallel Algebraic Multigrid Solver and Preconditioner,” *Applied Numerical Mathematics*, **41**, 1, 155 (2000); 10.1016/S0168-9274(01)00115-5.
- [17] H. DE STERCK, T. MANTEUFFEL, S. MCCORMICK, K. MILLER, J. PEARSON, J. RUGE, and G. SANDERS, “Smoothed Aggregation Multigrid for Markov Chains,” *SIAM Journal on Scientific Computing*, **32**, 1, 40 (2010); 10.1137/080719157.
- [18] T. A. MANTEUFFEL, L. N. OLSON, J. B. SCHRODER, and B. S. SOUTHWORTH, “A Root-Node Based Algebraic Multigrid Method,” *arXiv:1610.03154 [math]* (2016).
- [19] D. A. KNOLL, H. PARK, and C. NEWMAN, “Acceleration of K -Eigenvalue/Criticality Calculations Using the Jacobian-Free Newton-Krylov Method,” *Nuclear Science and Engineering*, **167**, 2, 133 (2011); dx.doi.org/10.13182/NSE09-89.

- [20] M. A. SMITH, E. E. LEWIS, and B.-C. NA, “Benchmark on Deterministic 2-D MOX Fuel Assembly Transport Calculations without Spatial Homogenization,” *Progress in Nuclear Energy*, **45**, 2, 107 (2004).
- [21] C. N. MCGRAW, M. L. ADAMS, W. D. HAWKINS, M. P. ADAMS, and T. SMITH, “Accuracy of the Linear Discontinuous Galerkin Method for 3D Reactor Analysis with Resolved Fuel Pins,” *Mathematics and Computations, Supercomputing in Nuclear Applications and Monte Carlo International Conference, M and C+SNA+MC 2015*, vol. 4, 3155–3168, American Nuclear Society (2015).
- [22] Y. WANG, M. D. DEHART, D. R. GASTON, F. N. GLEICHER, R. C. MARTINEAU, J. ORTENSI, J. W. PETERSON, and S. SCHUNERT, “Convergence Study of Rattlesnake Solutions for the Two-Dimensional C5G7 Mox Benchmark,” *Mathematics and Computations, Supercomputing in Nuclear Applications and Monte Carlo International Conference, M and C+SNA+MC 2015*, vol. 4, 2881–2892, American Nuclear Society (2015).
- [23] J. R. SHEWCHUK, “Triangle: Engineering a 2D Quality Mesh Generator and Delaunay Triangulator,” *Applied Computational Geometry towards Geometric Engineering*, 203–222, Springer.
- [24] “Idaho National Laboratory | TOP500 Supercomputer Sites,” <https://www.top500.org/site/47650> (2017).